INTERNATIONAL JOURNAL FOR NUMERICAL METHODS IN FLUIDS, VOL. 15, 841–863 (1992)

A QUADRATIC-ELEMENT FORMULATION OF THE COMPLEX VARIABLE BOUNDARY ELEMENT METHOD

ROBERT T. BAILEY

Westinghouse Savannah River Technology Center, P.O. Box 616, Aiken, SC 29802, U.S.A.

AND

C. K. HSIEH

Department of Mechanical Engineering, University of Florida, Gainesville, FL 32611, U.S.A.

SUMMARY

The complex variable boundary element method (CVBEM) for simply connected domains is extended to include the use of quadratic elements and interpolating functions. The derivation follows the format for linear elements given in the literature, with second-degree Lagrange polynomials taken as the interpolating functions. The quadratic-element CVBEM nodal- and interior-point equations are given in detail, and the resulting formulation is successfully tested by solving example problems with available analytical solutions. Comparisons of computational efficiency and accuracy are made between the solutions obtained using linear and quadratic elements. Additional comparisons are made using published results from other boundary element methods.

KEY WORDS Boundary elements Complex variables CVBEM

INTRODUCTION

Over the past decade, the boundary element methods (BEMs) have been developed to supplement the well-established finite-difference methods (FDMs) and finite-element methods (FEMs) in the numerical solution of partial differential equations (PDEs).[1,2] In fact, in certain situations, it has been shown that the BEMs can be more computationally efficient and more accurate than the FDMs or FEMs, particularly in the solution of Laplace's or Poisson's equations.[1–6] Traditionally, the BEMs have been formulated using real variables (RVBEMs), but a recent and powerful advance involves the use of complex variables, the result being a method known as the complex variable boundary element method (CVBEM).[7] In either type of BEM, the computational dimension is one less than the physical dimension. That is, a problem posed in a domain is reduced to finding the solution on the boundary. As for comparison between the two methods, the CVBEM is limited in application to Laplace's and Poisson's equations, and is further limited to two-dimensional (2D) domains (while the RVBEMs are not), but it does possess the following two significant advantages over the RVBEMs: (1) the expressions for calculating the values of the potential at points on the interior of the domain are analytic and satisfy exactly the 2D Laplace equation and (2) all integrations are carried out analytically without the need for numerical integration. These factors combine to give the CVBEM excellent potential for both high accuracy and efficiency.

0271–2091/92/200841–23$16.50

Received 17 September 1991
Revised 8 May 1992

The origins of the CVBEM can be traced to a paper by Hunt and Issacs,[8] where it was applied to the solution of groundwater flow problems. Hromadka and Guymon[9] subsequently used the method to predict freezing fronts in soils and then formalized the rather loose development into the CVBEM.[10] The method was also shown by Hromadka[11] to be a generalization of the analytic function method of Van Der Veer.[12] In the process of refining the CVBEM, Hromadka[13] developed a technique for error visualization at the domain boundary and determined relative error bounds for the method.[14] He also considered the use of variable trial functions for improving accuracy[15] and investigated the proper placement of collocation points on the domain boundary.[16]

Various physical phenomena have been modelled by the CVBEM, including groundwater contaminant transport,[8,17,18] conduction heat transfer,[16] prediction of freezing fronts in soil,[9,19] and stratified flows.[20] All these applications and developments have been detailed in a book on the CVBEM by Hromadka and Lai;[7] however, more recent developments in the CVBEM (post-1987) are not covered in this book. The CVBEM has since been extended from simply connected to doubly and multiply connected domains by Kassab,[21] Kassab and Hsieh,[22] and Hsieh and Kassab.[23] It was found that the complex potential along cuts in the domain does not cancel out, but results in a complex stream function that plays the role of a perturbation in the nodal equations. About the same time, Harryman *et al.*[24] and Hromadka[25] applied the CVBEM to specific multiply connected domains where such perturbations did not appear due to a zero-flux condition on the interior boundaries. More recently, Mokry[26] has applied the CVBEM to external potential flows. Examples were given for flows over aerofoils whose exact solutions are known. In all cases, the agreement of the CVBEM results with the theory was excellent.

In the CVBEM development reviewed above, only constant or linear boundary elements were utilized. The use of complex variable cubic splines in conjunction with the CVBEM has been demonstrated by Homentcovschi and Kreindler.[27] Comparisons were made with the integral equation method of Symm[28] for the conformal mapping of a bounded simply connected domain onto a unit disk. In general, the cubic-spline results possessed errors smaller than those of Symm by an order of magnitude.

As one might expect, the jump from linear elements to cubic splines introduced significant complexities into the CVBEM formulation. Quadratic elements would offer a compromise between the linear and cubic-spline approaches, and the foundation for their use in the CVBEM has been laid by Hromadka[7] via generalized proofs. Nevertheless, quadratic elements have never been attempted. It is, therefore, the purpose of this paper to present a quadratic-element formulation of the CVBEM for simply connected domains.

DERIVATION OF THE FUNDAMENTAL CVBEM EQUATIONS USING QUADRATIC ELEMENTS

The formulation of the quadratic-element CVBEM begins with Cauchy's integral formula,

$$\omega(z_0)=\frac{1}{2\pi i}\int_\Gamma \frac{\omega(\zeta)}{\zeta-z_0}\,d\zeta, \quad z_0\in\Omega,\ z_0\notin\Gamma. \tag{1}$$

This expression relates the value of the complex potential, $\omega=\phi+i\psi$, at point z_0 located inside the k-connected Jordan domain, Ω, to a contour integral (containing ω) along the boundary, Γ. Here, ϕ represents the real potential and ψ represents the stream function. The direction of travel for the contour integral is such that the interior of the domain is always to the left.

The quadratic-element formulation of the CVBEM transforms the Cauchy integral formula into a BEM by using two major approximations. First, the boundary Γ is discretized into M finite-length curved elements, Γ_j. These elements are formed by passing a quadratic polynomial through three successive nodal points. The domain boundary is taken as the union of these elements, as shown in Figure 1, i.e.

$$\Gamma = \bigcup_{j=1}^{M} \Gamma_j. \tag{2}$$

Note that the element j contains nodes k, $k+1$, and $k+2$, so that the indices j and k are related by $k=2j-1$. Further, M elements are formed from $N=2M$ nodal points.

In the second approximation, the function $\omega(z)$ is replaced by a quadratic global trial function, $G_2(z)$, given by

$$G_2(z) = \sum_{\substack{j=1 \\ k=2j-1}}^{M} M_k(z)\,\omega_k + M_{k+1}(z)\,\omega_{k+1} + M_{k+2}(z)\,\omega_{k+2}, \tag{3}$$

where ω_k, ω_{k+1}, and ω_{k+2} represent the complex potential ω at nodal points z_k, z_{k+1}, and z_{k+2}, respectively, and $M_k(z)$, $M_{k+1}(z)$, and $M_{k+2}(z)$ are continuous basis functions weighting the effects of ω_k, ω_{k+1}, and ω_{k+2} over elements Γ_{j-1} and Γ_j. These basis functions are taken as

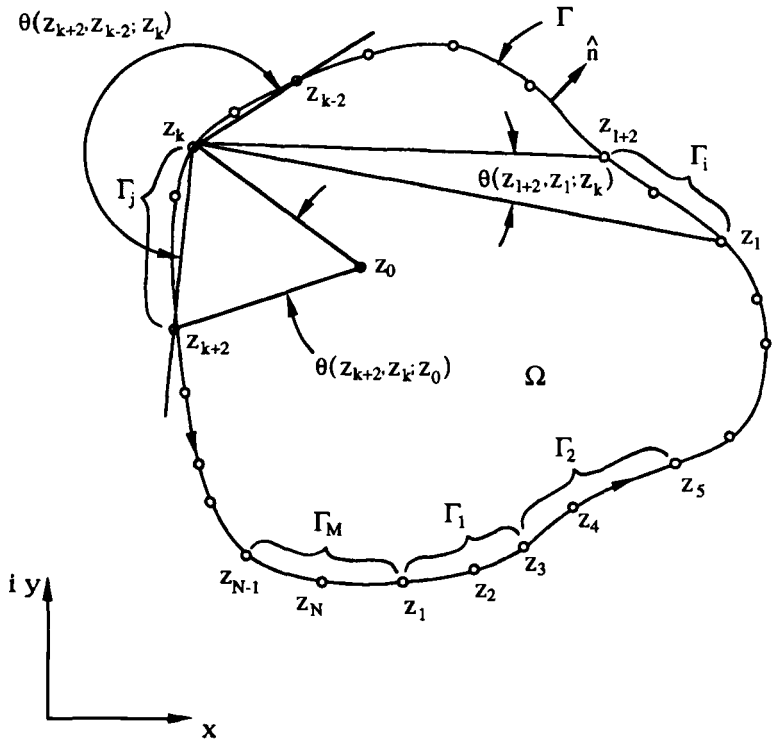

Figure 1. Boundary discretization and angle definitions in the quadratic-element CVBEM

second-degree Lagrange polynomials of the form

$$M_k(z)=\begin{cases}\dfrac{(z-z_{k-2})\,(z-z_{k-1})}{(z_k-z_{k-2})\,(z_k-z_{k-1})}, & z\in\Gamma_{j-1},\\[2ex] \dfrac{(z_{k+1}-z)\,(z_{k+2}-z)}{(z_k-z_{k+2})\,(z_k-z_{k+1})}, & z\in\Gamma_j,\\[2ex] 0, & z\notin\Gamma_{j-1}\cup\Gamma_j.\end{cases} \tag{4}$$

It is necessary to explain the notation that will be used in this paper. The subscript exact will identify a quantity whose value is known exactly. The overbar will refer to a quantity whose value is specified, such as in the boundary conditions. Finally, the hat will represent a quantity whose value is treated as an unknown in the solution by the CVBEM. Quantities with such designations missing should be assumed to represent a general case in which the quantity in question may be either specified or unknown, depending upon the circumstances.

By substituting $G_2(\zeta)$ for $\omega(\zeta)$ on the right-hand side of the Cauchy integral formula [equation (1)], the second-order CVBEM approximation of ω can be expressed as

$$\hat{\omega}(z_0)=\frac{1}{2\pi i}\int_\Gamma \frac{G_2(\zeta)}{\zeta-z_0}\,d\zeta, \quad z_0\in\Omega,\ z_0\notin\Gamma. \tag{5}$$

After much simplification (see Appendix I), the contour integral can be eliminated, and the above equation reduces to

$$\hat{\omega}_0=\hat{\omega}(z_0)=\frac{1}{2\pi i}\sum_{\substack{j=1\\ k=2j-1}}^{M} C_k\omega_k+C_{k+1}\,\omega_{k+1}+C_{k+2}\,\omega_{k+2}, \tag{6a}$$

where

$$C_k=\left\{\frac{(z_{k+2}z_{k+1})(z_{k+2}-z_{k+1})h_k}{D}-\frac{(z_{k+2}+z_{k+1})(z_{k+2}-z_{k+1})[(z_{k+2}-z_k)+z_0h_k]}{D}\right.$$
$$\left.+\frac{(z_{k+2}-z_{k+1})\{(z_{k+2}^2-z_k^2)/2+z_0[(z_{k+2}-z_k)+z_0h_k]\}}{D}\right\}, \tag{6b}$$

$$C_{k+1}=\left\{\frac{-(z_{k+2}z_k)(z_{k+2}-z_k)h_k}{D}+\frac{(z_{k+2}+z_k)(z_{k+2}-z_k)[(z_{k+2}-z_k)+z_0h_k]}{D}\right.$$
$$\left.-\frac{(z_{k+2}-z_k)\{(z_{k+2}^2-z_k^2)/2+z_0[(z_{k+2}-z_k)+z_0h_k]\}}{D}\right\}, \tag{6c}$$

$$C_{k+2}=\left\{\frac{(z_{k+1}z_k)(z_{k+1}-z_k)h_k}{D}-\frac{(z_{k+1}+z_k)(z_{k+1}-z_k)[(z_{k+2}-z_k)+z_0h_k]}{D}\right.$$
$$\left.+\frac{(z_{k+1}-z_k)\{(z_{k+2}^2-z_k^2)/2+z_0[(z_{k+2}-z_k)+z_0h_k]\}}{D}\right\}, \tag{6d}$$

$$D=(z_{k+2}-z_k)(z_{k+1}-z_k)(z_{k+2}-z_{k+1}), \tag{6e}$$

$$h_k=\ln\left[\frac{(z_{k+2}-z_0)}{(z_k-z_0)}\right]=\ln\left|\frac{(z_{k+2}-z_0)}{(z_k-z_0)}\right|+i\theta(z_{k+2},z_k;z_0). \tag{6f}$$

This formula forms the basis for the quadratic-element CVBEM. [See Figure 1 for the definition of $\theta(z_{k+2}, z_k; z_0)$.]

Equation (6), being expressed in complex variables, actually embodies two equations—one for the real part and one for the imaginary part. These equations are given by

$$\hat{\phi}_0 = \hat{\phi}(z_0) = \frac{1}{2\pi}\left[\sum_{\substack{j=1 \\ k=2j-1}}^{M} (C_k^{\mathrm{I}}\phi_k + C_k^{\mathrm{R}}\psi_k + C_{k+1}^{\mathrm{I}}\phi_{k+1} + C_{k+1}^{\mathrm{R}}\psi_{k+1} + C_{k+2}^{\mathrm{I}}\phi_{k+2} + C_{k+2}^{\mathrm{R}}\psi_{k+2}) \right] \tag{7}$$

and

$$\hat{\psi}_0 = \hat{\psi}(z_0) = -\frac{1}{2\pi}\left[\sum_{\substack{j=1 \\ k=2j-1}}^{M} (C_k^{\mathrm{R}}\phi_k - C_k^{\mathrm{I}}\psi_k + C_{k+1}^{\mathrm{R}}\phi_{k+1} - C_{k+1}^{\mathrm{I}}\psi_{k+1} + C_{k+2}^{\mathrm{R}}\phi_{k+2} - C_{k+2}^{\mathrm{I}}\psi_{k+2}) \right]. \tag{8}$$

Here, the superscripts R and I refer to the real and imaginary parts, respectively.

If the values of ϕ and ψ (and, thus, ω) are known at each boundary node, equation (6) can be used to calculate $\hat{\omega}$ at any interior point, z_0. A close inspection reveals that this equation can also be used to calculate the value of $\hat{\omega}$ at the 'middle' node of any boundary element, Γ_j, i.e. for z_0 at z_{k+1}. In most potential problems, however, boundary conditions specify either ϕ (a Dirichlet condition) or ψ (a stream function condition), but not both. To solve for the unknown values of ϕ and ψ at the 'end' nodes along the boundary, i.e. for z_0 at z_k, it is necessary to derive an extended version of equation (6) by moving z_0 to the position of z_k on the boundary. In this effort, one cannot simply plug in z_k for z_0 in equation (6) because $z_k - z_0$ appears in the denominator of the natural log term. Instead, one takes the limit of equation (5) as z_0 approaches z_k. The result, as derived in Appendix II, is

$$\hat{\omega}_k = \hat{\omega}(z_k) = \frac{1}{2\pi \mathrm{i}}\,(F_{k-2}\omega_{k-2} + F_{k-1}\omega_{k-1} + F_k\omega_k + F_{k+1}\omega_{k+1} + F_{k+2}\omega_{k+2} + \sum_{\substack{i=1 \\ i,i+1\neq j \\ k=2j-1 \\ l=2i-1}}^{M} C_l\omega_l + C_{l+1}\omega_{l+1} + C_{l+2}\omega_{l+2}), \tag{9a}$$

where

$$F_{k-2} = \left[\frac{z_k - 2z_{k-1} + z_{k-2}}{2(z_{k-1} - z_{k-2})} \right], \tag{9b}$$

$$F_{k-1} = \left[\frac{-(z_k - z_{k-2})^2}{2(z_k - z_{k-1})(z_{k-1} - z_{k-2})} \right], \tag{9c}$$

$$F_k = \left[\ln\left|\frac{(z_{k+2} - z_k)}{(z_{k-2} - z_k)}\right| + \mathrm{i}\theta(z_{k+2}, z_{k-2}; z_k) + \frac{3z_k - 2z_{k-1} - z_{k-2}}{2(z_k - z_{k-1})} - \frac{3z_k - 2z_{k+1} - z_{k+2}}{2(z_k - z_{k+1})} \right], \tag{9d}$$

$$F_{k+1} = \left[\frac{(z_k - z_{k+2})^2}{2(z_k - z_{k+1})(z_{k+1} - z_{k+2})} \right], \tag{9e}$$

$$F_{k+2} = \left[\frac{-z_k + 2z_{k+1} - z_{k+2}}{2(z_{k+1} - z_{k+2})} \right], \tag{9f}$$

$$C_l=\left\{\frac{(z_{l+2}z_{l+1})(z_{l+2}-z_{l+1})h_l}{D}-\frac{(z_{l+2}+z_{l+1})(z_{l+2}-z_{l+1})[(z_{l+2}-z_l)+z_kh_l]}{D}\right.$$
$$\left.+\frac{(z_{l+2}-z_{l+1})\{(z_{l+2}^2-z_l^2)/2+z_k[(z_{l+2}-z_l)+z_kh_l]\}}{D}\right\}, \tag{9g}$$

$$C_{l+1}=\left\{\frac{-(z_{l+2}z_l)(z_{l+2}-z_l)h_l}{D}+\frac{(z_{l+2}+z_l)(z_{l+2}-z_l)[(z_{l+2}-z_l)+z_kh_l]}{D}\right.$$
$$\left.-\frac{(z_{l+2}-z_l)\{(z_{l+2}^2-z_l^2)/2+z_k[(z_{l+2}-z_l)+z_kh_l]\}}{D}\right\}, \tag{9h}$$

$$C_{l+2}=\left\{\frac{(z_{l+1}z_l)(z_{l+1}-z_l)h_l}{D}-\frac{(z_{l+1}+z_l)(z_{l+1}-z_l)[(z_{l+2}-z_l)+z_kh_l]}{D}\right.$$
$$\left.+\frac{(z_{l+1}-z_l)\{(z_{l+2}^2-z_l^2)/2+z_k[(z_{l+2}-z_l)+z_kh_l]\}}{D}\right\}, \tag{9i}$$

$$D=(z_{l+2}-z_l)(z_{l+1}-z_l)(z_{l+2}-z_{l+1}), \tag{9j}$$

$$h_l=\ln\left[\frac{(z_{l+2}-z_k)}{(z_l-z_k)}\right]=\ln\left|\frac{(z_{l+2}-z_k)}{(z_l-z_k)}\right|+\mathrm{i}\theta(z_{l+2},z_l;z_k). \tag{9k}$$

See Figure 1 for the definition of $\theta(z_{k+2}, z_{k-2}; z_k)$ and $\theta(z_{l+2}, z_l; z_k)$.

Equation (9) can be applied at any end boundary node, but like equation (6), equation (9) has real and imaginary parts. Two equations can, thus, be derived for any end boundary node k as

$$\hat{\phi}_k=\hat{\phi}(z_k)=\frac{1}{2\pi}\left[F_{k-2}^{\mathrm{I}}\phi_{k-2}+F_{k-2}^{\mathrm{R}}\psi_{k-2}+F_{k-1}^{\mathrm{I}}\phi_{k-1}+F_{k-1}^{\mathrm{R}}\psi_{k-1}\right.$$
$$+F_k^{\mathrm{I}}\phi_k+F_k^{\mathrm{R}}\psi_k+F_{k+1}^{\mathrm{I}}\phi_{k+1}+F_{k+1}^{\mathrm{R}}\psi_{k+1}+F_{k+2}^{\mathrm{I}}\phi_{k+2}+F_{k+2}^{\mathrm{R}}\psi_{k+2}$$
$$\left.+\sum_{\substack{i=1\\ i,i+1\neq j\\ k=2j-1\\ l=2i-1}}^{M}(C_l^{\mathrm{I}}\phi_l+C_l^{\mathrm{R}}\psi_l+C_{l+1}^{\mathrm{I}}\phi_{l+1}+C_{l+1}^{\mathrm{R}}\psi_{l+1}+C_{l+2}^{\mathrm{I}}\phi_{l+2}+C_{l+2}^{\mathrm{R}}\psi_{l+2})\right] \tag{10}$$

and

$$\hat{\psi}_k=\hat{\psi}(z_k)=-\frac{1}{2\pi}\left[F_{k-2}^{\mathrm{R}}\phi_{k-2}-F_{k-2}^{\mathrm{I}}\psi_{k-2}+F_{k-1}^{\mathrm{R}}\phi_{k-1}-F_{k-1}^{\mathrm{I}}\psi_{k-1}\right.$$
$$+F_k^{\mathrm{R}}\phi_k-F_k^{\mathrm{I}}\psi_k+F_{k+1}^{\mathrm{R}}\phi_{k+1}-F_{k+1}^{\mathrm{I}}\psi_{k+1}+F_{k+2}^{\mathrm{R}}\phi_{k+2}-F_{k+2}^{\mathrm{I}}\psi_{k+2}$$
$$+\sum_{\substack{i=1\\ i,i+1\neq j\\ k=2j-1\\ l=2i-1}}^{M}(C_l^{\mathrm{R}}\phi_l-C_l^{\mathrm{I}}\psi_l+C_{l+1}^{\mathrm{R}}\phi_{l+1}-C_{l+1}^{\mathrm{I}}\psi_{l+1}$$
$$\left.+C_{l+2}^{\mathrm{R}}\phi_{l+2}-C_{l+2}^{\mathrm{I}}\psi_{l+2})\right]. \tag{11}$$

As in equations (7) and (8), the superscripts R and I refer to the real and imaginary parts, respectively. Complete expressions for these real and imaginary parts are given in Reference 29.

SOLUTION METHODS

Equations (7), (8), (10) and (11) will be used to estimate the unknown values of ϕ and ψ at the boundary nodes. Prior to the presentation of the methodology for this estimation, a close examination of these equations is in order. It is clear from their format that $\hat{\phi}$ and $\hat{\psi}$ on the left can be calculated by using the known values of ϕ and ψ at all boundary nodes whose indices appear on the right. As discussed previously, some of the values of ϕ and ψ at the boundary nodes are not specified by the boundary conditions. The methods for estimating the unspecified values of ϕ and ψ (designated $\hat{\phi}$ and $\hat{\psi}$), thus, hinge on how these quantities are related to the specified quantities ($\bar{\phi}$ and $\bar{\psi}$) and on which of the equations [(7), (8), (10) or (11)] is used in the construction of the matrix equation for the solution of the problem. Two sets of methods are developed, depending upon the location of the nodal point in the boundary element—one set for end boundary nodes and one set for middle boundary nodes.

Nodal point at one end of element

For a nodal point that is located at one end of a boundary element (e.g. z_k of Γ_j in Figure 1), where a Dirichlet (ϕ-specified) or stream function (ψ-specified) condition is imposed, there are three methods of solving for the estimated nodal values of $\hat{\phi}_k$ or $\hat{\psi}_k$.

Explicit method. For a Dirichlet condition imposed at end node k, ϕ_k is known (as $\bar{\phi}_k$) but ψ_k is not. One, thus, sets $\hat{\phi}_k = \phi_k = \bar{\phi}_k$ and $\psi_k = \hat{\psi}_k$. The first setting is governed by the fact that a Dirichlet condition is specified; no estimation is, thus, needed for ϕ_k. The second setting is made in order to estimate the unknown value of ψ_k. Without such a setting, there will be two unknowns (ψ_k and $\hat{\psi}_k$) at the same nodal point, a situation which does not allow for a unique solution. Since the field theory predicts that the estimated $\hat{\psi}_k$, if error-free, should be exactly equal to that imposed, equating ψ_k and $\hat{\psi}_k$ is certainly justifiable.

In the explicit method, an effort is made to keep all the unknowns on the right-hand side of the equation. It is, therefore, impossible to use equation (11) since $\hat{\psi}_k$ on the left-hand side is unknown for the Dirichlet condition specified. Thus, equation (10) is used as

$$\begin{aligned}\bar{\phi}_k = -\frac{1}{2\pi}\Bigg[& F^{\mathrm{I}}_{k-2}\phi_{k-2} + F^{\mathrm{R}}_{k-2}\psi_{k-2} + F^{\mathrm{I}}_{k-1}\phi_{k-1} + F^{\mathrm{R}}_{k-1}\psi_{k-1} \\ & + F^{\mathrm{I}}_{k}\bar{\phi}_k + F^{\mathrm{R}}_{k}\hat{\psi}_k + F^{\mathrm{I}}_{k+1}\phi_{k+1} + F^{\mathrm{R}}_{k+1}\psi_{k+1} + F^{\mathrm{I}}_{k+2}\phi_{k+2} + F^{\mathrm{R}}_{k+2}\psi_{k+2} \\ & + \sum_{\substack{i=1 \\ i,i+1\neq j \\ k=2j-1 \\ l=2i-1}}^{M} (C^{\mathrm{I}}_{l}\phi_l + C^{\mathrm{R}}_{l}\psi_l + C^{\mathrm{I}}_{l+1}\phi_{l+1} + C^{\mathrm{R}}_{l+1}\psi_{l+1} + C^{\mathrm{I}}_{l+2}\phi_{l+2} + C^{\mathrm{R}}_{l+2}\psi_{l+2}) \Bigg]. \end{aligned} \tag{12}$$

For the explicit method, it is sufficient to use equation (12) to solve for $\hat{\psi}_k$. Equation (11) is dropped.

For a stream function condition at node k, ψ_k is known (as $\bar{\psi}_k$) but ϕ_k is not. One, thus, sets $\hat{\psi}_k = \psi_k = \bar{\psi}_k$ and $\phi_k = \hat{\phi}_k$. This time, for the explicit method of solution, equation (11) is used, and

the nodal equation is

$$\bar{\psi}_k = -\frac{1}{2\pi}\Bigg[F^{\mathrm{R}}_{k-2}\phi_{k-2} - F^{\mathrm{I}}_{k-2}\psi_{k-2} + F^{\mathrm{R}}_{k-1}\phi_{k-1} - F^{\mathrm{I}}_{k-1}\psi_{k-1} + F^{\mathrm{R}}_{k}\hat{\phi}_k - F^{\mathrm{I}}_{k}\bar{\psi}_k + F^{\mathrm{R}}_{k+1}\phi_{k+1} - F^{\mathrm{I}}_{k+1}\psi_{k+1} + F^{\mathrm{R}}_{k+2}\phi_{k+2} - F^{\mathrm{I}}_{k+2}\psi_{k+2} + \sum_{\substack{i=1 \\ i,i+1\neq j \\ k=2j-1 \\ l=2i-1}}^{M} (C^{\mathrm{R}}_{l}\phi_l - C^{\mathrm{I}}_{l}\psi_l + C^{\mathrm{R}}_{l+1}\phi_{l+1} - C^{\mathrm{I}}_{l+1}\psi_{l+1} + C^{\mathrm{R}}_{l+2}\phi_{l+2} - C^{\mathrm{I}}_{l+2}\psi_{l+2}) \Bigg]. \tag{13}$$

Equation (10) is dropped for this node in the solution.

Implicit method. For a Dirichlet condition imposed at end node k, one sets $\phi_k = \bar{\phi}_k$ and $\psi_k = \hat{\psi}_k$. However, unlike the explicit method, the implicit method involves a nodal equation where unknowns appear on both sides. Equation (11) is, thus, used as

$$\hat{\psi}_k = -\frac{1}{2\pi}\Bigg[F^{\mathrm{R}}_{k-2}\phi_{k-2} - F^{\mathrm{I}}_{k-2}\psi_{k-2} + F^{\mathrm{R}}_{k-1}\phi_{k-1} - F^{\mathrm{I}}_{k-1}\psi_{k-1} + F^{\mathrm{R}}_{k}\bar{\phi}_k - F^{\mathrm{I}}_{k}\hat{\psi}_k + F^{\mathrm{R}}_{k+1}\phi_{k+1} - F^{\mathrm{I}}_{k+1}\psi_{k+1} + F^{\mathrm{R}}_{k+2}\phi_{k+2} - F^{\mathrm{I}}_{k+2}\psi_{k+2} + \sum_{\substack{i=1 \\ i,i+1\neq j \\ k=2j-1 \\ l=2i-1}}^{M} (C^{\mathrm{R}}_{l}\phi_l - C^{\mathrm{I}}_{l}\psi_l + C^{\mathrm{R}}_{l+1}\phi_{l+1} - C^{\mathrm{I}}_{l+1}\psi_{l+1} + C^{\mathrm{R}}_{l+2}\phi_{l+2} - C^{\mathrm{I}}_{l+2}\psi_{l+2}) \Bigg]. \tag{14}$$

Equation (10) is dropped.

Similarly, for a stream function condition specified at end node k, one sets $\psi_k = \bar{\psi}_k$ and $\phi_k = \hat{\phi}_k$. Equation (10) is now used as

$$\hat{\phi}_k = \frac{1}{2\pi}\Bigg[F^{\mathrm{I}}_{k-2}\phi_{k-2} + F^{\mathrm{R}}_{k-2}\psi_{k-2} + F^{\mathrm{I}}_{k-1}\phi_{k-1} + F^{\mathrm{R}}_{k-1}\psi_{k-1} + F^{\mathrm{I}}_{k}\hat{\phi}_k + F^{\mathrm{R}}_{k}\bar{\psi}_k + F^{\mathrm{I}}_{k+1}\phi_{k+1} + F^{\mathrm{R}}_{k+1}\psi_{k+1} + F^{\mathrm{I}}_{k+2}\phi_{k+2} + F^{\mathrm{R}}_{k+2}\psi_{k+2} + \sum_{\substack{i=1 \\ i,i+1\neq j \\ k=2j-1 \\ l=2i-1}}^{M} (C^{\mathrm{I}}_{l}\phi_l + C^{\mathrm{R}}_{l}\psi_l + C^{\mathrm{I}}_{l+1}\phi_{l+1} - C^{\mathrm{R}}_{l+1}\psi_{l+1} + C^{\mathrm{I}}_{l+2}\phi_{l+2} + C^{\mathrm{R}}_{l+2}\psi_{l+2}) \Bigg]. \tag{15}$$

Equation (11) is dropped.

Hybrid method. For a Dirichlet condition imposed at end node k, one sets $\hat{\phi}_k = \bar{\phi}_k$ on the left-hand side of equation (10) and $\phi_k = \hat{\phi}_k$ and $\psi_k = \hat{\psi}_k$ on the right-hand sides of equations (10) and (11) to obtain

$$\bar{\phi}_k = \frac{1}{2\pi}\Bigg[F^{\mathrm{I}}_{k-2}\phi_{k-2} + F^{\mathrm{R}}_{k-2}\psi_{k-2} + F^{\mathrm{I}}_{k-1}\phi_{k-1} + F^{\mathrm{R}}_{k-1}\psi_{k-1} + F^{\mathrm{I}}_{k}\hat{\phi}_k + F^{\mathrm{R}}_{k}\hat{\psi}_k + F^{\mathrm{I}}_{k+1}\phi_{k+1} + F^{\mathrm{R}}_{k+1}\psi_{k+1} + F^{\mathrm{I}}_{k+2}\phi_{k+2} + F^{\mathrm{R}}_{k+2}\psi_{k+2} + \sum_{\substack{i=1 \\ i,i+1\neq j \\ k=2j-1 \\ l=2i-1}}^{M} (C^{\mathrm{I}}_{l}\phi_l + C^{\mathrm{R}}_{l}\psi_l + C^{\mathrm{I}}_{l+1}\phi_{l+1} + C^{\mathrm{R}}_{l+1}\psi_{l+1} + C^{\mathrm{I}}_{l+2}\phi_{l+2} + C^{\mathrm{R}}_{l+2}\psi_{l+2}) \Bigg], \tag{16}$$

$$\hat{\psi}_k = -\frac{1}{2\pi}\Bigg[F^{\mathrm{R}}_{k-2}\phi_{k-2} - F^{\mathrm{I}}_{k-2}\psi_{k-2} + F^{\mathrm{R}}_{k-1}\phi_{k-1} - F^{\mathrm{I}}_{k-1}\psi_{k-1} + F^{\mathrm{R}}_{k}\hat{\phi}_k - F^{\mathrm{I}}_{k}\hat{\psi}_k + F^{\mathrm{R}}_{k+1}\phi_{k+1} - F^{\mathrm{I}}_{k+1}\psi_{k+1} + F^{\mathrm{R}}_{k+2}\phi_{k+2} - F^{\mathrm{I}}_{k+2}\psi_{k+2} + \sum_{\substack{i=1 \\ i,i+1\neq j \\ k=2j-1 \\ l=2i-1}}^{M} (C^{\mathrm{R}}_l\phi_l - C^{\mathrm{I}}_l\psi_l + C^{\mathrm{R}}_{l+1}\phi_{l+1} - C^{\mathrm{I}}_{l+1}\psi_{l+1} + C^{\mathrm{R}}_{l+2}\phi_{l+2} - C^{\mathrm{I}}_{l+2}\psi_{l+2}) \Bigg]. \tag{17}$$

Note that in equations (16) and (17) both $\hat{\phi}_k$ and $\hat{\psi}_k$ are unknown.

For a stream function condition imposed at end node k, one sets $\hat{\psi}_k = \bar{\psi}_k$ on the left-hand side of equation (11) and $\psi_k = \hat{\psi}_k$ and $\phi_k = \hat{\phi}_k$ on the right-hand sides of equations (10) and (11) to yield

$$\hat{\phi}_k = \frac{1}{2\pi}\Bigg[F^{\mathrm{I}}_{k-2}\phi_{k-2} + F^{\mathrm{R}}_{k-2}\psi_{k-2} + F^{\mathrm{I}}_{k-1}\phi_{k-1} + F^{\mathrm{R}}_{k-1}\psi_{k-1} + F^{\mathrm{I}}_{k}\hat{\phi}_k + F^{\mathrm{R}}_{k}\hat{\psi}_k + F^{\mathrm{I}}_{k+1}\phi_{k+1} + F^{\mathrm{R}}_{k+1}\psi_{k+1} + F^{\mathrm{I}}_{k+2}\phi_{k+2} + F^{\mathrm{R}}_{k+2}\psi_{k+2} + \sum_{\substack{i=1 \\ i,i+1\neq j \\ k=2j-1 \\ l=2i-1}}^{M} (C^{\mathrm{I}}_l\phi_l + C^{\mathrm{R}}_l\psi_l + C^{\mathrm{I}}_{l+1}\phi_{l+1} + C^{\mathrm{R}}_{l+1}\psi_{l+1} + C^{\mathrm{I}}_{l+2}\phi_{l+2} + C^{\mathrm{R}}_{l+2}\psi_{l+2}) \Bigg], \tag{18}$$

$$\bar{\psi}_k = -\frac{1}{2\pi}\Bigg[F^{\mathrm{R}}_{k-2}\phi_{k-2} - F^{\mathrm{I}}_{k-2}\psi_{k-2} + F^{\mathrm{R}}_{k-1}\phi_{k-1} - F^{\mathrm{I}}_{k-1}\psi_{k-1} + F^{\mathrm{R}}_{k}\hat{\phi}_k - F^{\mathrm{I}}_{k}\hat{\psi}_k + F^{\mathrm{R}}_{k+1}\phi_{k+1} - F^{\mathrm{I}}_{k+1}\psi_{k+1} + F^{\mathrm{R}}_{k+2}\phi_{k+2} - F^{\mathrm{I}}_{k+2}\psi_{k+2} + \sum_{\substack{i=1 \\ i,i+1\neq j \\ k=2j-1 \\ l=2i-1}}^{M} (C^{\mathrm{R}}_l\phi_l - C^{\mathrm{I}}_l\psi_l + C^{\mathrm{R}}_{l+1}\phi_{l+1} - C^{\mathrm{I}}_{l+1}\psi_{l+1} + C^{\mathrm{R}}_{l+2}\phi_{l+2} - C^{\mathrm{I}}_{l+2}\psi_{l+2}) \Bigg]. \tag{19}$$

Again, both $\hat{\phi}_k$ and $\hat{\psi}_k$ are unknown.

Nodal point at the middle of element

At the middle nodal point $k+1$ (see Figure 1), where a Dirichlet (ϕ-specified) or stream function (ψ-specified) condition is imposed, the same three methods of solving for the estimated nodal values of $\hat{\phi}_{k+1}$ or $\hat{\psi}_{k+1}$ are possible. Point z_0 is now moved to z_{k+1} and the methods are detailed as follows.

Explicit method. For a Dirichlet condition imposed at the middle node $k+1$, one sets $\hat{\phi}_0 = \phi_{k+1} = \bar{\phi}_{k+1}$ and $\psi_{k+1} = \hat{\psi}_{k+1}$ in equation (7) as

$$\bar{\phi}_{k+1} = \frac{1}{2\pi}\Bigg[C^{\mathrm{I}}_k\phi_k + C^{\mathrm{R}}_k\psi_k + C^{\mathrm{I}}_{k+1}\bar{\phi}_{k+1} + C^{\mathrm{R}}_{k+1}\hat{\psi}_{k+1} + C^{\mathrm{I}}_{k+2}\phi_{k+2} + C^{\mathrm{R}}_{k+2}\psi_{k+2} + \sum_{\substack{i=1 \\ i\neq j \\ l=2i-1}}^{M} (C^{\mathrm{I}}_l\phi_l + C^{\mathrm{R}}_l\psi_l + C^{\mathrm{I}}_{l+1}\phi_{l+1} + C^{\mathrm{R}}_{l+1}\psi_{l+1} + C^{\mathrm{I}}_{l+2}\phi_{l+2} + C^{\mathrm{R}}_{l+2}\psi_{l+2}) \Bigg]. \tag{20}$$

Equation (8) is dropped.

For a stream function condition at the middle node $k+1$, one sets $\hat{\psi}_0=\psi_{k+1}=\bar{\psi}_{k+1}$ and $\phi_{k+1}=\hat{\phi}_{k+1}$ in equation (8) to yield

$$\bar{\psi}_{k+1}=-\frac{1}{2\pi}\Bigg[C_k^{\mathrm{R}}\phi_k-C_k^{\mathrm{I}}\psi_k+C_{k+1}^{\mathrm{R}}\hat{\phi}_{k+1}-C_{k+1}^{\mathrm{I}}\bar{\psi}_{k+1}+C_{k+2}^{\mathrm{R}}\phi_{k+2}-C_{k+2}^{\mathrm{I}}\psi_{k+2}+\sum_{\substack{i=1\\ i\neq j\\ l=2i-1}}^{M}(C_l^{\mathrm{R}}\phi_l-C_l^{\mathrm{I}}\psi_l+C_{l+1}^{\mathrm{R}}\phi_{l+1}-C_{l+1}^{\mathrm{I}}\psi_{l+1}+C_{l+2}^{\mathrm{R}}\phi_{l+2}-C_{l+2}^{\mathrm{I}}\psi_{l+2})\Bigg]. \tag{21}$$

Equation (7) is dropped for this node in the solution.

Implicit method. For a Dirichlet condition imposed at the middle node $k+1$, one sets $\phi_{k+1}=\bar{\phi}_{k+1}$ and $\hat{\psi}_0=\psi_{k+1}=\hat{\psi}_{k+1}$ in equation (8) as

$$\hat{\psi}_{k+1}=-\frac{1}{2\pi}\Bigg[C_k^{\mathrm{R}}\phi_k-C_k^{\mathrm{I}}\psi_k+C_{k+1}^{\mathrm{R}}\bar{\phi}_{k+1}-C_{k+1}^{\mathrm{I}}\hat{\psi}_{k+1}+C_{k+2}^{\mathrm{R}}\phi_{k+2}-C_{k+2}^{\mathrm{I}}\psi_{k+2}+\sum_{\substack{i=1\\ i\neq j\\ l=2i-1}}^{M}(C_l^{\mathrm{R}}\phi_l-C_l^{\mathrm{I}}\psi_l+C_{l+1}^{\mathrm{R}}\phi_{l+1}-C_{l+1}^{\mathrm{I}}\psi_{l+1}+C_{l+2}^{\mathrm{R}}\phi_{l+2}-C_{l+2}^{\mathrm{I}}\psi_{l+2})\Bigg]. \tag{22}$$

Equation (7) is dropped.

Similarly, for a stream function condition specified at the middle node $k+1$, one sets $\psi_{k+1}=\bar{\psi}_{k+1}$ and $\hat{\phi}_0=\phi_{k+1}=\hat{\phi}_{k+1}$. Equation (7) is now used as

$$\hat{\phi}_{k+1}=\frac{1}{2\pi}\Bigg[C_k^{\mathrm{I}}\phi_k+C_k^{\mathrm{R}}\psi_k+C_{k+1}^{\mathrm{I}}\hat{\phi}_{k+1}+C_{k+1}^{\mathrm{R}}\bar{\psi}_{k+1}+C_{k+2}^{\mathrm{I}}\phi_{k+2}+C_{k+2}^{\mathrm{R}}\psi_{k+2}+\sum_{\substack{i=1\\ i\neq j\\ l=2i-1}}^{M}(C_l^{\mathrm{I}}\phi_l+C_l^{\mathrm{R}}\psi_l+C_{l+1}^{\mathrm{I}}\phi_{l+1}+C_{l+1}^{\mathrm{R}}\psi_{l+1}+C_{l+2}^{\mathrm{I}}\phi_{l+2}+C_{l+2}^{\mathrm{R}}\psi_{l+2})\Bigg]. \tag{23}$$

Equation (8) is dropped.

Hybrid method. For a Dirichlet condition imposed at the middle node $k+1$, one sets $\hat{\phi}_0=\bar{\phi}_{k+1}$ and $\hat{\psi}_0=\hat{\psi}_{k+1}$ on the left-hand sides of equations (7) and (8) and $\phi_{k+1}=\hat{\phi}_{k+1}$ and $\psi_{k+1}=\hat{\psi}_{k+1}$ on the right-hand sides of these equations to obtain

$$\bar{\phi}_{k+1}=\frac{1}{2\pi}\Bigg[C_k^{\mathrm{I}}\phi_k+C_k^{\mathrm{R}}\psi_k+C_{k+1}^{\mathrm{I}}\hat{\phi}_{k+1}+C_{k+1}^{\mathrm{R}}\hat{\psi}_{k+1}+C_{k+2}^{\mathrm{I}}\phi_{k+2}+C_{k+2}^{\mathrm{R}}\psi_{k+2}+\sum_{\substack{i=1\\ i\neq j\\ l=2i-1}}^{M}(C_l^{\mathrm{I}}\phi_l+C_l^{\mathrm{R}}\psi_l+C_{l+1}^{\mathrm{I}}\phi_{l+1}+C_{l+1}^{\mathrm{R}}\psi_{l+1}+C_{l+2}^{\mathrm{I}}\phi_{l+2}+C_{l+2}^{\mathrm{R}}\psi_{l+2})\Bigg], \tag{24}$$

$$\hat{\psi}_{k+1}=-\frac{1}{2\pi}\Bigg[C_k^{\mathrm{R}}\phi_k-C_k^{\mathrm{I}}\psi_k+C_{k+1}^{\mathrm{R}}\hat{\phi}_{k+1}-C_{k+1}^{\mathrm{I}}\hat{\psi}_{k+1}+C_{k+2}^{\mathrm{R}}\phi_{k+2}-C_{k+2}^{\mathrm{I}}\psi_{k+2}+\sum_{\substack{i=1\\ i\neq j\\ l=2i-1}}^{M}(C_l^{\mathrm{R}}\phi_l-C_l^{\mathrm{I}}\psi_l+C_{l+1}^{\mathrm{R}}\phi_{l+1}-C_{l+1}^{\mathrm{I}}\psi_{l+1}+C_{l+2}^{\mathrm{R}}\phi_{l+2}-C_{l+2}^{\mathrm{I}}\psi_{l+2})\Bigg], \tag{25}$$

Note that both $\hat{\phi}_{k+1}$ and $\hat{\psi}_{k+1}$ are unknown.

For a stream function condition imposed at node $k+1$, one sets $\hat{\phi}_0=\hat{\phi}_{k+1}$ and $\hat{\psi}_0=\bar{\psi}_{k+1}$ on the left-hand sides of equations (7) and (8) and $\psi_{k+1}=\hat{\psi}_{k+1}$ and $\phi_{k+1}=\hat{\phi}_{k+1}$ on the right-hand sides of these equations to yield

$$\hat{\phi}_{k+1}=\frac{1}{2\pi}\left[C_k^{\mathrm{I}}\phi_k+C_k^{\mathrm{R}}\psi_k+C_{k+1}^{\mathrm{I}}\hat{\phi}_{k+1}+C_{k+1}^{\mathrm{R}}\hat{\psi}_{k+1}+C_{k+2}^{\mathrm{I}}\phi_{k+2}+C_{k+2}^{\mathrm{R}}\psi_{k+2} + \sum_{\substack{i=1\\ i\neq j\\ l=2i-1}}^{M} (C_l^{\mathrm{I}}\phi_l+C_l^{\mathrm{R}}\psi_l+C_{l+1}^{\mathrm{I}}\phi_{l+1}+C_{l+1}^{\mathrm{R}}\psi_{l+1}+C_{l+2}^{\mathrm{I}}\phi_{l+2}+C_{l+2}^{\mathrm{R}}\psi_{l+2}) \right]. \tag{26}$$

$$\bar{\psi}_{k+1}=-\frac{1}{2\pi}\left[C_k^{\mathrm{R}}\phi_k-C_k^{\mathrm{I}}\psi_k+C_{k+1}^{\mathrm{R}}\hat{\phi}_{k+1}-C_{k+1}^{\mathrm{I}}\hat{\psi}_{k+1}+C_{k+2}^{\mathrm{R}}\phi_{k+2}-C_{k+2}^{\mathrm{I}}\psi_{k+2} + \sum_{\substack{i=1\\ i\neq j\\ l=2i-1}}^{M} (C_l^{\mathrm{R}}\phi_l-C_l^{\mathrm{I}}\psi_l+C_{l+1}^{\mathrm{R}}\phi_{l+1}-C_{l+1}^{\mathrm{I}}\psi_{l+1}+C_{l+2}^{\mathrm{R}}\phi_{l+2}-C_{l+2}^{\mathrm{I}}\psi_{l+2}) \right]. \tag{27}$$

Again, both $\hat{\phi}_{k+1}$ and $\hat{\psi}_{k+1}$ are unknown.

For the explicit method, equation (12) is applied at each Dirichlet end node, equation (13) at each stream function end node, equation (20) at each Dirichlet middle node, and equation (21) at each stream function middle node. Similarly, for the implicit method, one applies equation (14) at each Dirichlet end node, equation (15) at each stream function end node, equation (22) at each Dirichlet middle node, and equation (23) at each stream function middle node. Finally, in the hybrid method, equations (16) and (17) are applied at each Dirichlet end mode, equations (18) and (19) at each stream function end node, equations (24) and (25) at each Dirichlet middle node, and equations (26) and (27) at each stream function middle node. In all three cases, a system of simultaneous linear algebraic equations is obtained. This system can be represented in a matrix form as

$$\mathbf{C}\begin{Bmatrix}\hat{\phi}\\ \hat{\psi}\end{Bmatrix}=\mathbf{r}. \tag{28}$$

Here, $\mathbf{C}$ is the square matrix of coefficients on the unknown values of $\hat{\phi}$ and $\hat{\psi}$ and $\mathbf{r}$ is a vector of known constants. The system can be solved by any direct method such as Gaussian elimination with scaled partial pivoting. Once the unknown values of $\hat{\phi}$ and $\hat{\psi}$ are found at each boundary node, one can use these values, together with the specified values, $\bar{\phi}$ and $\bar{\psi}$, as the boundary nodal values needed by equation (6) for calculating $\hat{\omega}$ at any interior point.

Calculation of the normal gradient of the potential

After ϕ and ψ have been evaluated at the boundary nodes, the values of ψ may be used to determine $\partial\phi/\partial n$ at these nodes. Use is made of the Cauchy–Riemann conditions,

$$\frac{\partial\phi}{\partial n}=\frac{\partial\psi}{\partial s}, \tag{29}$$

where n is now taken as the outward normal to Γ with s as its tangential co-ordinate, assumed positive in the direction of the contour integral in equation (1). The partial differential $\partial\psi/\partial s$ (and, thus, $\partial\phi/\partial n$) can be approximated by using finite-difference formulae. For example, a second-order-accurate, three-point backward finite-difference approximation to $\partial\psi/\partial s$ at node i is given

by

$$\left(\frac{\partial \psi}{\partial s}\right)_i = \frac{\psi_i[(s_i - s_{i-2})^2 - (s_i - s_{i-1})^2] - \psi_{i-1}(s_i - s_{i-2})^2}{(s_i - s_{i-1})(s_i - s_{i-2})(s_{i-1} - s_{i-2})} + \frac{\psi_{i-2}(s_i - s_{i-1})^2}{(s_i - s_{i-1})(s_i - s_{i-2})(s_{i-1} - s_{i-2})}. \tag{30}$$

The values of the tangential arc length, s, can be estimated as the cumulative sum of the lengths of the linear segments connecting each successive nodal point, or a more sophisticated polynomial or spline procedure may be used. One-sided formulae should be used at corner nodes and at any others where the normal gradients are different on either side of the node. Central-differencing can be used at all the remaining nodes. Equations such as (30) can be greatly simplified if the nodal points are equally spaced along the boundary, and References 30 and 31 provide lists of some common finite-difference formulae which can be used when this is the case.

Additional comments and the psi reference node

Two more points are worthy of note. First, the implicit method is preferred over the explicit and hybrid methods for reasons detailed in References 7 and 29. Second, no matter what boundary conditions exist, one must specify a reference value of ψ at some nodal point along the boundary in order to serve as the constant of integration in equation (5). Numerically speaking, the associated matrices become singular if no ψ value is provided. This anchor node will be referred to as the 'psi reference node'. Numbering it as node i, one has

$$\bar{\psi}_i = \psi_{\text{exact},i}.$$

Equation (15) or (23) (depending upon whether node i is a middle or end node) can then be used to determine the unknown $\hat{\phi}_i$, as was discussed earlier in the description of the implicit method.

If, however, the value of ϕ_{exact} is also known at node i (i.e. a Dirichlet condition), one can specify both $\bar{\phi}$ and $\bar{\psi}$ at this node as

$$\bar{\phi}_i = \phi_{\text{exact},i}$$

and

$$\bar{\psi}_i = \psi_{\text{exact},i}.$$

The complex potential ω is, thus, fully specified, and no nodal equation needs to be applied. This node will be called a 'completely specified node'.

EXAMPLES

The quadratic-element formulation of the CVBEM was tested by application to the circular domain shown in Figure 2. Two separate complex potential distributions were assumed, namely

$$\omega = z^2, \tag{31}$$

which results in

$$\phi = x^2 - y^2, \tag{32}$$

$$\psi = 2xy, \tag{33}$$

$$\frac{\partial \phi}{\partial n} = 2[x\cos(\theta) - y\sin(\theta)] \tag{34}$$

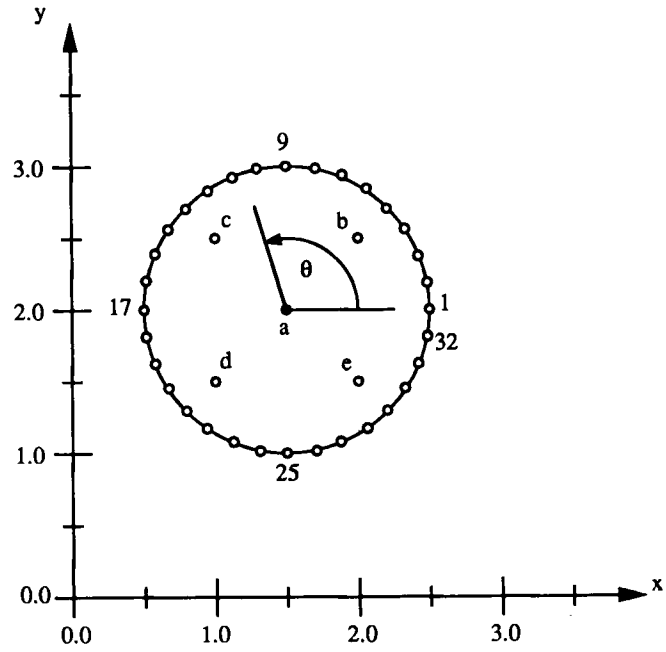

Figure 2. The circular domain used to test the quadratic-element CVBEM

and

$$\omega = e^z, \tag{35}$$

which results in

$$\phi = \exp(x)\cos(y), \tag{36}$$

$$\psi = \exp(x)\sin(y), \tag{37}$$

$$\frac{\partial \phi}{\partial n} = \exp(x)[\cos(y)\cos(\theta) - \sin(y)\sin(\theta)]. \tag{38}$$

For both distributions, Dirichlet boundary conditions were specified at all 32 boundary nodes (including node 1, which was treated as a completely specified node). The stream function and normal gradient of the potential were then calculated at each node using both the linear-element and the quadratic-element CVBEM. Also, ϕ and ψ were calculated at five internal points labelled a–e in Figure 2.

The quadratic-element CVBEM was also tested on a series of five problems considered earlier by Symm[28] and Homentcovschi and Kreindler.[27] These problems involve the conformal mapping of the region bounded by the ellipse

$$\frac{x^2}{a^2} + y^2 = 1 \tag{39}$$

to the unit disk $|W| \leqslant 1$ in the complex plane in such a way that the point $z_0 = 0$ is mapped to $W = 0$. Five different values of a were considered—1·25, 2·5, 5·0, 10·0, and 20·0.

The mapping itself is given by

$$W = z \exp[\omega(z)], \tag{40}$$

where $\omega(z)$ was determined based on the Dirichlet boundary condition

$$\phi = -\ln|z|, \quad z \in \Gamma \tag{41}$$

imposed at 32 equally spaced nodes along the boundary, Γ, of the ellipse.

As in References 27 and 28, an estimate of the maximum error in the modulus of W was calculated using

$$\mathrm{EM} = \max_k ||W(z_{k+1/2})| - 1| \qquad (k = 1, 2, \ldots, N). \tag{42}$$

The intermediate points, $z_{k+1/2}$, were taken to lie half-way between nodes z_k and z_{k+1} along the boundary.

Finally, as a more practical example in the area of fluid flow, the quadratic-element CVBEM was applied to the problem of potential flow over a circular cylinder. Taking advantage of symmetry, only one-quarter of the total domain is considered, as shown in Figure 3. The analytical solution is given by

$$\omega = z + \frac{1}{z}. \tag{43}$$

The above expression could have been used to generate Dirichlet conditions at the boundaries, but since the objective of this example was to provide a somewhat realistic application for the

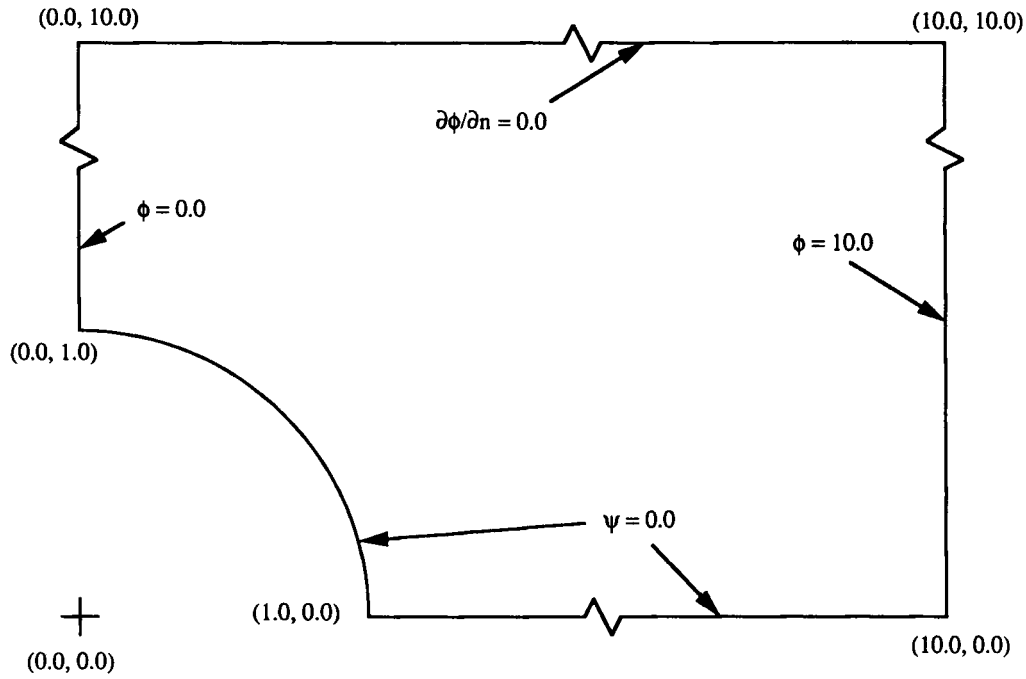

Figure 3. Geometry and boundary conditions for potential flow over a circular cylinder

method, the more physical boundary conditions shown in Figure 3 were imposed. The $\phi = 10{\cdot}0$ condition on the right boundary and the $\partial\phi/\partial n = 0{\cdot}0$ condition at the top are approximations; however, it was determined that the error induced in the solution due to these approximations was relatively small (less than 1 per cent).

A total of 30 nodal points were used—seven on the circular arc and on each of the four linear boundaries. (This sums to 35, but the five corner nodes common to two boundary segments are double-counted.) The nodes on the same segment were equally spaced, but spacing varied between segments, depending upon the length of each segment. Node 1 was placed at location (0·0, 1·0), and the numbering proceeded counterclockwise around the boundary. (Thus, the double-counted nodes are 1, 7, 13, 19 and 25.) The unspecified values of ϕ and ψ were calculated at each of the 30 nodes using the linear-element and quadratic-element formulations of the CVBEM. The locations of representative streamlines in the interior of the domain were also calculated.

All the examples in this paper were solved by using either a 33 MHz 80386 based personal computer equipped with a 33 MHz 80387 math co-processor or a 12 MHz 80286 based personal computer fixed with an 8 MHz 80287 math co-processor. The computer codes themselves were written in Turbo Pascal Version 4·0. Two major programs were written—one for the linear-element CVBEM and one for the quadratic-element CVBEM—along with several minor programs for data creation.

RESULTS AND DISCUSSION

The distribution given by equation (31) was chosen specifically because ω is quadratic in z. Therefore, the solutions obtained using quadratic elements should be exact (except for roundoff errors). This was indeed the case, with the values of ϕ and ψ at both the boundary nodes and interior points being accurate to at least 14 decimal places. The results for $\partial\phi/\partial n$ at the boundary, while not exact, were also good, with a maximum percentage error of 0·59 at nodal point 17 and a mean error of 0·18 per cent over all the boundary nodes. Some error in $\partial\phi/\partial n$ was expected since $\partial\phi/\partial n$ is not quadratic, as can be seen from equation (34).

The exponential distribution given by equation (35) was chosen to provide a comparison between the solutions obtained using the linear-element and quadratic-element formulations of the CVBEM. The results for the percentage error in ψ and $\partial\phi/\partial n$ at the boundary nodes for this distribution are given in Figures 4 and 5, respectively. It is noted that the percentage error in $\partial\phi/\partial n$ at the boundary is a good upper bound on the overall error in the computation for two reasons. First, in the CVBEM, $\partial\phi/\partial n$ must be calculated from the nodal values of ψ using finite-difference formulae. This makes $\partial\phi/\partial n$ generally less accurate than either ϕ or ψ. Second, quantities at the boundary which are not specified by the boundary conditions tend to be less accurate than those calculated at interior points. In fact, in the numerical solution of potential problems, the maximum error in the estimated values of ϕ and ψ occurs on the boundary.[7]

As shown in Figures 4 and 5, the errors at each of the nodal points were reduced significantly by the use of the quadratic elements, with the maximum percentage error in $\partial\phi/\partial n$ being 13·74 for the linear elements and 3·79 for the quadratic elements, an almost threefold improvement. The results at the interior points are given in Table I, and a similar improvement in the accuracy due to the quadratic elements is apparent.

The computational times for the linear- and quadratic-element solutions referred to in Figures 4 and 5 were 19 and 35 s, respectively, on an 80286/80287 based personal computer. However, it was found that a quadratic-element solution using only 16 equally spaced nodes still possessed

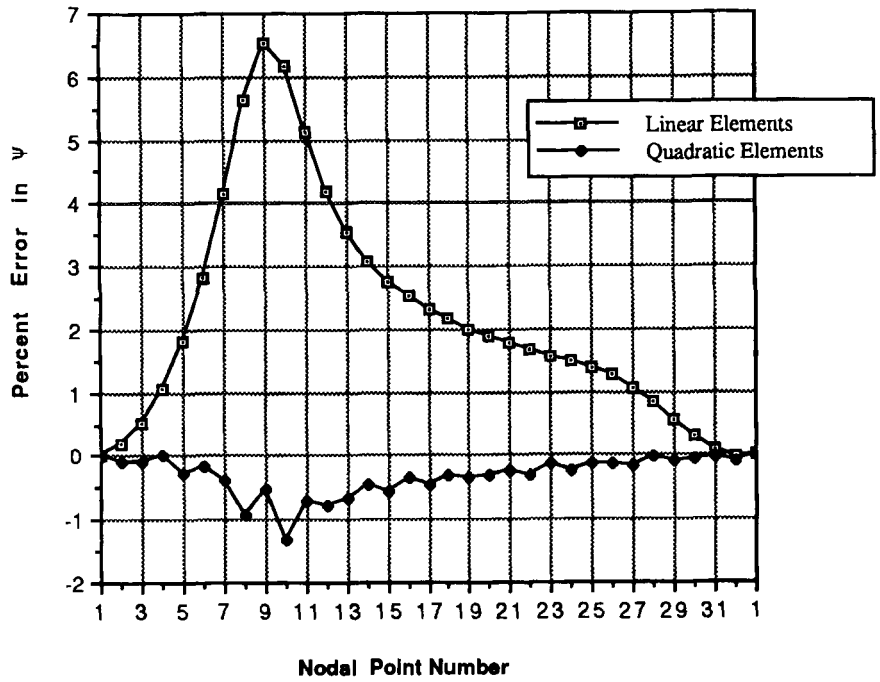

Figure 4. Percentage error in the stream function at the boundary nodes of the domain shown in Figure 2 in comparison with the complex potential given by equation (35)

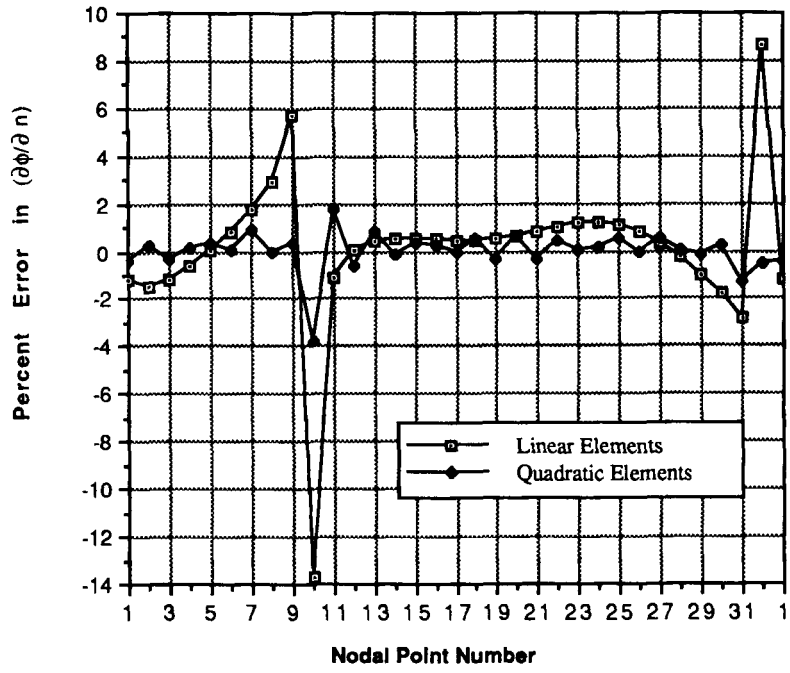

Figure 5. Percentage error in the normal gradient of the potential at the boundary nodes of the domain shown in Figure 2 in comparison with the complex potential given by equation (35)

Table I. The percentage error in ϕ and ψ at the interior points for the CVBEM solution on the domain of Figure 2 in comparison with the complex potential of equation (35)

	Linear elements		Quadratic elements	
Interior point	Percentage error in ϕ	Percentage error in ψ	Percentage error in ϕ	Percentage error in ψ
a	0·00	−0·98	0·00	0·142
b	0·18	−1·23	−0·002	0·123
c	−0·18	−2·11	0·005	0·354
d	−3·46	−1·45	0·054	·0·216
e	3·48	−0·56	0·044	0·075

Table II. The error EM [see equation (42)] in the solution of the conformal mapping of five different ellipses [see Equation (39)] onto the unit disk by four different methods

	EM			
a	Symm[28]	Linear-element CVBEM	Quadratic-element CVBEM	Cubic-spline CVBEM[27]
1·25	$6·0 \times 10^{-4}$	$1·2 \times 10^{-3}$	$3·2 \times 10^{-5}$	$5·4 \times 10^{-6}$
2·5	$6·5 \times 10^{-3}$	$1·5 \times 10^{-2}$	$2·5 \times 10^{-3}$	$4·3 \times 10^{-4}$
5·0	$5·0 \times 10^{-2}$	$5·9 \times 10^{-2}$	$2·9 \times 10^{-2}$	$1·0 \times 10^{-3}$
10·0	0·2116	0·1382	0·1068	$6·1 \times 10^{-2}$
20·0	0·4878	0·2111	0·1989	0·31

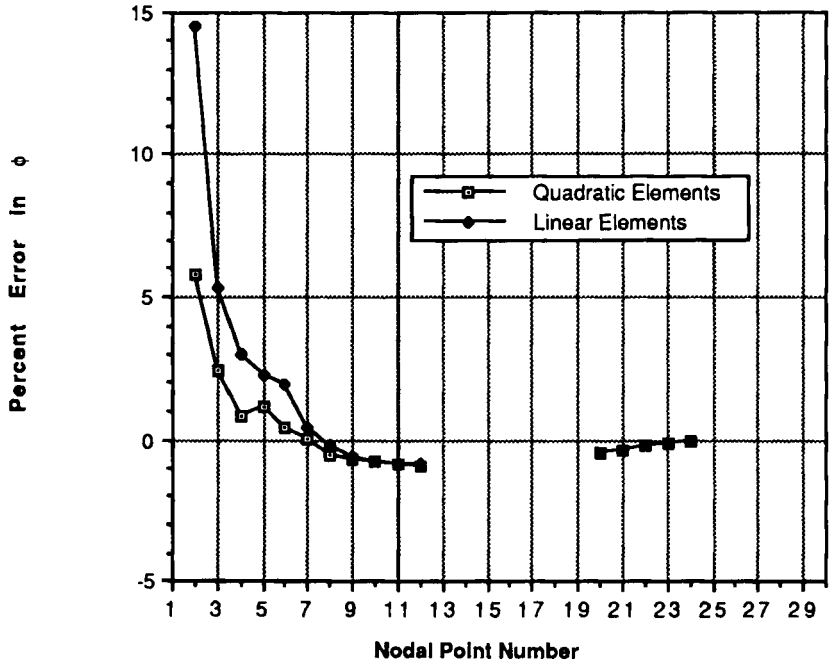

Figure 6. Percentage error in the unspecified values of the potential at the boundary nodes of the domain shown in Figure 3

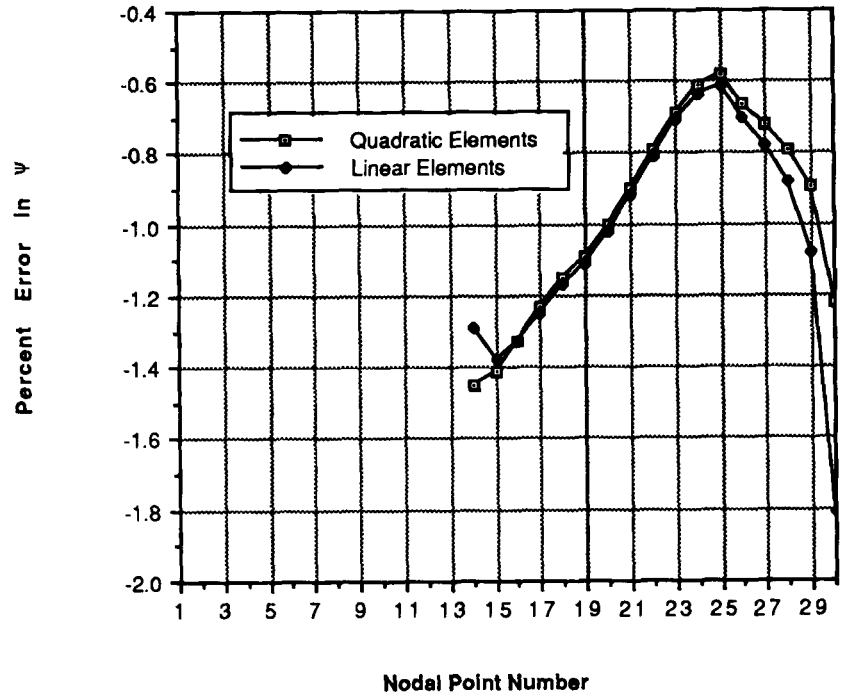

Figure 7. Percentage error in the unspecified values of the stream function at the boundary nodes of the domain shown in Figure 3

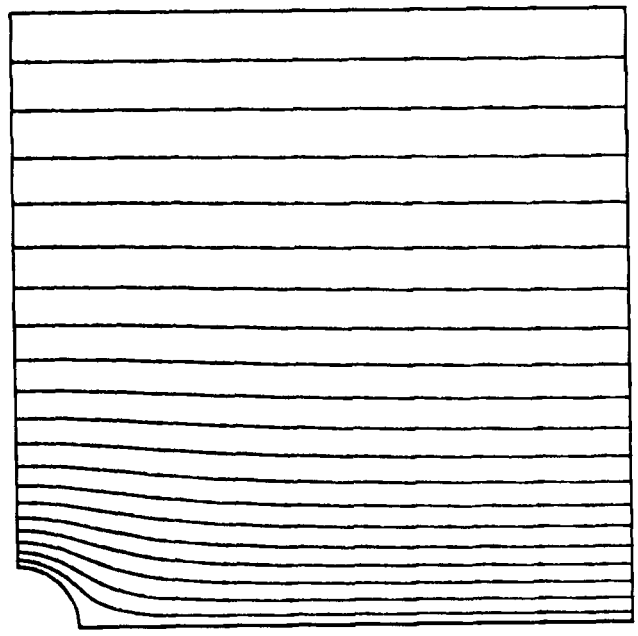

Figure 8. Streamlines in the domain of Figure 3 as calculated by the quadratic-element CVBEM

a smaller maximum error in $\partial\phi/\partial n$ than the 32-node linear-element solution. The run-time for this 16-node quadratic-element solution was 11 s.

Table II shows the error, EM, for the five conformal mapping cases described earlier. The results are presented for a constant-element RVBEM,[28] the linear-element CVBEM, the quadratic-element CVBEM, and the cubic-spline CVBEM.[27] In all the cases, the results obtained using the quadratic-element CVBEM are better than those of Symm or the linear-element CVBEM, and they compare well with those obtained using the cubic-spline CVBEM. Indeed, for $a = 20{\cdot}0$, the quadratic-element results are more accurate than the spline results. Comparisons of computational time between the quadratic-element and cubic-spline methods were not made since no information on execution times was provided in Reference 27.

Finally, CVBEM results for flow over a circular cylinder are given in Figures 6–8. Figures 6 and 7 show the percentage error in the unspecified values of ϕ and ψ, respectively, at the boundary nodes. As with the circular domain results discussed previously, the quadratic-element solution was significantly more accurate, with a maximum percentage error in ϕ of 5·81 for the quadratic elements compared to 14·49 for the linear elements. A plot of the interior streamlines as calculated by the quadratic-element CVBEM is shown in Figure 8.

CLOSING REMARKS

A word regarding the use of quadratic elements versus simply adding more nodal points with linear elements is in order. Although the examples presented in this paper involved relatively few nodes (< 40), it is reasonable to propose that there would be a point where the addition of nodal points would raise the computing time to an unacceptable level. Gaussian elimination with scaled partial pivoting—the method chosen here for the solution of matrix equation (28)—is an N^3 algorithm, meaning that the computational time increases roughly as the cube of the number of equations (nodes). Further, as the number of equations was increased, accuracy limitations associated with direct solution methods (such as Gaussian elimination) would be exposed. Thus, there would be a practical limit to the number of nodes allowed for accuracy. Iterative methods (such as conjugate gradient methods), although not as susceptible to roundoff error, would still suffer the same limitations regarding computational time. Therefore, in cases where computer resources are limited, either in terms of speed, precision, or storage, quadratic elements can provide high accuracy with modest hardware (such as a personal computer).

Another point which is worthy of discussion is the utility of the CVBEM in general. In today's CFD arena filled with exotic turbulence models and hypersonic chemically reacting flows simulations, it is legitimate to ask whether another method for solving Laplace's (or Poisson's) equation is really worth considering. It is the authors' feeling that the versatile engineer carries with him or her a variety of numerical tools—choosing the appropriate tool for each particular application. The CVBEM is one such specialized but highly efficient tool that can handle complex boundaries in two dimensions with relative ease. It is an excellent candidate for use as a potential flow solver in a 2D viscous/inviscid interaction code. The ability to calculate values at any interior-point location once the boundary values are fully determined is a valuable feature that the CVBEM shares with all BEMs, since it allows the resolution of the interior flow field to be adjusted without re-solving the entire problem.

In summary, a quadratic-element formulation of the CVBEM for simply connected domains has been presented. Previously, the linear-element CVBEM has been shown to be an effective numerical method for obtaining solutions to a broad range of potential problems, and a formulation using cubic splines has also been presented in the literature. The quadratic-element CVBEM developed herein was found to produce more accurate results than its linear-element counterpart

and compared well with the cubic-spline formulation. Although only Dirichlet and stream function boundary conditions were considered here, Neumann and Robin conditions can also be handled as described in References 21 and 29. It should be mentioned, however, that the inclusion of Neumann or Robin boundary conditions can lead to complications at boundary corners—an issue which has been resolved in Reference 32. Finally, since the linear-element CVBEM has been extended to the solution of problems in multiply connected domains, the quadratic-element CVBEM can be extended in this manner as well.

APPENDIX I

In this appendix, the steps required to transform equation (5) into equation (6) will be presented. By using equations (3) and (4), the contour integral in equation (5) is first rewritten as

$$\int_\Gamma \frac{G_2(\zeta)}{\zeta - z_0}\,d\zeta = \sum_{\substack{j=1 \\ k=2j-1}}^{M} \int_{\Gamma_j} \left[\frac{(z_{k+1}-\zeta)(z_{k+2}-\zeta)}{(z_{k+1}-z_k)(z_{k+2}-z_k)}\omega_k + \frac{(\zeta - z_k)(z_{k+2}-\zeta)}{(z_{k+1}-z_k)(z_{k+2}-z_{k+1})}\omega_{k+1} + \frac{(\zeta - z_k)(\zeta - z_{k+1})}{(z_{k+2}-z_k)(z_{k+2}-z_{k+1})}\omega_{k+2} \right] \frac{d\zeta}{\zeta - z_0}. \tag{44}$$

By expanding out the product terms, grouping like powers of ζ, and pulling all constants out of the resulting contour integrals, equation (44) becomes

$$\begin{aligned} \int_\Gamma \frac{G_2(\zeta)}{\zeta - z_0}\,d\zeta = \sum_{\substack{j=1 \\ k=2j-1}}^{M} & \left[\frac{(z_{k+1}z_{k+2})\omega_k}{(z_{k+1}-z_k)(z_{k+2}-z_k)} - \frac{(z_k z_{k+2})\omega_{k+1}}{(z_{k+1}-z_k)(z_{k+2}-z_{k+1})} + \frac{(z_k z_{k+1})\omega_{k+2}}{(z_{k+2}-z_k)(z_{k+2}-z_{k+1})} \right] \int_{\Gamma_j} \frac{d\zeta}{\zeta - z_0} \\ & \times \left[\frac{-(z_{k+2}+z_{k+1})\omega_k}{(z_{k+1}-z_k)(z_{k+2}-z_k)} + \frac{(z_{k+2}+z_k)\omega_{k+1}}{(z_{k+1}-z_k)(z_{k+2}-z_{k+1})} + \frac{-(z_k+z_{k+1})\omega_{k+2}}{(z_{k+2}-z_k)(z_{k+2}-z_{k+1})} \right] \int_{\Gamma_j} \frac{\zeta\,d\zeta}{\zeta - z_0} \\ & \times \left[\frac{\omega_k}{(z_{k+1}-z_k)(z_{k+2}-z_k)} + \frac{\omega_{k+1}}{(z_{k+1}-z_k)(z_{k+2}-z_{k+1})} + \frac{\omega_{k+2}}{(z_{k+2}-z_k)(z_{k+2}-z_{k+1})} \right] \int_{\Gamma_j} \frac{\zeta^2\,d\zeta}{\zeta - z_0}. \end{aligned} \tag{45}$$

The three contour integrals on the right-hand of equation (45) can now be evaluated analytically as follows:

$$\int_{\Gamma_j} \frac{d\zeta}{\zeta - z_0} = \ln\left[\frac{(z_{k+2}-z_0)}{(z_k - z_0)}\right] = \ln\left|\frac{(z_{k+2}-z_0)}{(z_k-z_0)}\right| + i\theta(z_{k+2}, z_k; z_0) = h_k, \tag{46}$$

$$\int_{\Gamma_j} \frac{\zeta\,d\zeta}{\zeta - z_0} = (z_{k+2}-z_k) + z_0 h_k, \tag{47}$$

$$\int_{\Gamma_j} \frac{\zeta^2\,d\zeta}{\zeta - z_0} = \frac{(z_{k+2}^2 - z_k^2)}{2} + z_0\,[(z_{k+2}-z_k) + z_0 h_k]. \tag{48}$$

By substituting equations (46)–(48) into equation (45), finding a common denominator, grouping

the coefficients on ω_k, ω_{k+1}, and ω_{k+2}, and substituting the entire result back into equation (5), the desired interior-point equation, equation (6), is obtained.

APPENDIX II

This appendix presents the derivation of the quadratic-element CVBEM end-nodal equation—equation (9). In this effort, one takes the limit of equation (5) as z_0 approaches z_k (see Figure 1). To facilitate the limit process, equation (5) is first rewritten as

$$2\pi i\hat{\omega}(z_0)=\int_{\Gamma_{j-1}}\frac{G_2(\zeta)}{\zeta-z_0}\,d\zeta+\int_{\Gamma_j}\frac{G_2(\zeta)}{\zeta-z_0}\,d\zeta+\sum_{\substack{i=1\\ i\neq j\\ i\neq j-1}}^{M}\int_{\Gamma_i}\frac{G_2(\zeta)}{\zeta-z_0}\,d\zeta \tag{49}$$

so that the elements containing nodal point z_k (elements $j-1$ and j) may be treated separately. Using equations (45)–(48), equation (49) can be rewritten as

$$\begin{aligned}
2\pi i\hat{\omega}(z_0)=&\frac{\omega_{k-2}}{(z_k-z_{k-2})(z_{k-1}-z_{k-2})}\\
&\times\Big\{(z_{k-1}z_k)[\ln(z_k-z_0)-\ln(z_{k-2}-z_0)]-(z_k+z_{k-1})(z_k-z_{k-2})\\
&\quad-(z_k+z_{k-1})z_0[\ln(z_k-z_0)-\ln(z_{k-2}-z_0)]\\
&\quad+\frac{(z_k^2-z_{k-2}^2)}{2}+z_0(z_k-z_{k-2})+z_0^2[\ln(z_k-z_0)-\ln(z_{k-2}-z_0)]\Big\}\\
&+\frac{\omega_{k-1}}{(z_k-z_{k-1})(z_{k-1}-z_{k-2})}\\
&\times\Big\{-(z_{k-2}z_k)[\ln(z_k-z_0)-\ln(z_{k-2}-z_0)]+(z_k+z_{k-2})(z_k-z_{k-2})\\
&\quad+(z_k+z_{k-2})z_0[\ln(z_k-z_0)-\ln(z_{k-2}-z_0)]\\
&\quad-\frac{(z_k^2-z_{k-2}^2)}{2}-z_0(z_k-z_{k-2})-z_0^2[\ln(z_k-z_0)-\ln(z_{k-2}-z_0)]\Big\}\\
&+\frac{\omega_k}{(z_k-z_{k-2})(z_k-z_{k-1})}\\
&\times\Big\{(z_{k-2}z_{k-1})[\ln(z_k-z_0)-\ln(z_{k-2}-z_0)]-(z_{k-2}+z_{k-1})(z_k-z_{k-2})\\
&\quad-(z_{k-2}+z_{k-1})z_0[\ln(z_k-z_0)-\ln(z_{k-2}-z_0)]\\
&\quad+\frac{(z_k^2-z_{k-2}^2)}{2}+z_0(z_k-z_{k-2})+z_0^2[\ln(z_k-z_0)-\ln(z_{k-2}-z_0)]\Big\}\\
&+\frac{\omega_k}{(z_{k+2}-z_k)(z_{k+1}-z_k)}\\
&\times\Big\{(z_{k+1}z_{k+2})[\ln(z_{k+2}-z_0)-\ln(z_k-z_0)]-(z_{k+2}+z_{k+1})(z_{k+2}-z_k)\\
&\quad-(z_{k+2}+z_{k+1})z_0[\ln(z_{k+2}-z_0)-\ln(z_k-z_0)]
\end{aligned}$$

$$+\frac{(z_{k+2}^2-z_k^2)}{2}+z_0(z_{k+2}-z_k)+z_0^2[\ln(z_{k+2}-z_0)-\ln(z_k-z_0)]\Bigg\}$$

$$+\frac{\omega_{k+1}}{(z_{k+1}-z_k)(z_{k+2}-z_{k+1})}$$

$$\times\Bigg\{-(z_kz_{k+2})[\ln(z_{k+2}-z_0)-\ln(z_k-z_0)]+(z_{k+2}+z_k)(z_{k+2}-z_k)$$

$$+(z_{k+2}+z_k)z_0[\ln(z_{k+2}-z_0)-\ln(z_k-z_0)]$$

$$-\frac{(z_{k+2}^2-z_k^2)}{2}-z_0(z_{k+2}-z_k)-z_0^2[\ln(z_{k+2}-z_0)-\ln(z_k-z_0)]\Bigg\}$$

$$+\frac{\omega_{k+2}}{(z_{k+2}-z_k)(z_{k+2}-z_{k+1})}$$

$$\times\Bigg\{(z_kz_{k+1})[\ln(z_{k+2}-z_0)-\ln(z_k-z_0)]-(z_k+z_{k+1})(z_{k+2}-z_k)$$

$$-(z_k+z_{k+1})z_0[\ln(z_{k+2}-z_0)-\ln(z_k-z_0)]$$

$$+\frac{(z_{k+2}^2-z_k^2)}{2}+z_0(z_{k+2}-z_k)+z_0^2[\ln(z_{k+2}-z_0)-\ln(z_k-z_0)]\Bigg\}$$

$$+\sum_{\substack{i=1\\ i\neq j\\ i\neq j-1}}^{M}\int_{\Gamma_i}\frac{G_2(\zeta)}{\zeta-z_0}\,\mathrm{d}\zeta. \tag{50}$$

Now, taking the limit as z_0 approaches z_k in equation (50) yields

$$2\pi\mathrm{i}\,\hat{\omega}_k=\omega_{k-2}\left[\frac{z_k-2z_{k-1}+z_{k-2}}{2(z_{k-1}-z_{k-2})}\right]+\omega_{k-1}\left[\frac{-(z_k-z_{k-2})^2}{2(z_k-z_{k-1})(z_{k-1}-z_{k-2})}\right]$$

$$+\omega_k\left\{\ln\left[\frac{(z_{k+2}-z_k)}{(z_{k-2}-z_k)}\right]+\frac{3z_k-2z_{k-1}-z_{k-2}}{2(z_k-z_{k-1})}-\frac{3z_k-2z_{k+1}-z_{k+2}}{2(z_k-z_{k+1})}\right\}$$

$$+\omega_{k+1}\left[\frac{(z_k-z_{k+2})^2}{2(z_k-z_{k+1})(z_{k+1}-z_{k+2})}\right]+\omega_{k+2}\left[\frac{-z_k+2z_{k+1}-z_{k+2}}{2(z_{k+1}-z_{k+2})}\right]$$

$$+\sum_{\substack{i=1\\ i\neq j\\ i\neq j-1}}^{M}\int_{\Gamma_i}\frac{G_2(\zeta)}{\zeta-z_0}\,\mathrm{d}\zeta. \tag{51}$$

By utilizing equation (6) and introducing a more compact notation, equation (51) becomes the desired nodal equation, equation (9).

REFERENCES

1. P. K. Banerjee and R. Butterfield, *Boundary Element Methods in Engineering Science*, McGraw-Hill, London, 1981.
2. C. A. Brebbia and J. Dominguez, *Boundary Elements: An Introductory Course*, Computational Mechanics Publications, Boston, and McGraw-Hill, New York, 1989.
3. P. Bettess, 'Operation counts for boundary integral and finite element methods', *Int. j. numer. methods eng.*, **17**, 306–308 (1981).
4. S. Mukherjee and M. Morjaria, 'Comparison of boundary element and finite element methods in the inelastic torsion of prismatic shafts', *Int. j. numer. methods eng.*, **17**, 1576–1588 (1981).

5. S. Mukherjee and M. Morjaria, 'On the efficiency and accuracy of the boundary element method and the finite element method', *Int. j. numer. methods eng.*, **20**, 515–522 (1984).
6. E. C. Hume III, R. A. Brown and W. M. Deen, 'Comparison of boundary and finite element methods for moving boundary problems governed by a potential', *Int. j. numer. methods eng.*, **21**, 1295–1314 (1985).
7. T. V. Hromadka II and C. Lai, *The Complex Variable Boundary Element Method in Engineering Analysis*, Springer, New York, 1987.
8. G. Hunt and L. T. Issacs, 'Intergral equation formulation for ground-water flow', *J. Hydraul. Div.*, ASCE, **107**, 1197–1209 (1981).
9. T. V. Hromadka II and G. L. Guymon, 'Application of a boundary integral equation to prediction of freezing fronts in soil', *Cold Regions Sci. Technol.*, **6**, 115–121 (1982).
10. T. V. Hromadka II and G. L. Guymon, 'A complex variable boundary element method: development', *Int. j. numer. methods eng.*, **20**, 25–37 (1984).
11. T. V. Hromadka II, 'Linking the complex variable boundary element method to the analytic function method', *Numer. Heat Transfer*, **7**, 235–240 (1984).
12. P. Van Der Veer, 'Calculation methods for two-dimensional groundwater flow', Rijkswaterstaat Communications, No. 28/1978, Government Publishing Office, The Hague, The Netherlands, 1978.
13. T. V. Hromadka II, 'The complex variable boundary element method: development of approximative boundaries', *Eng. Analysis*, **1**(4), 218–222 (1984).
14. T. V. Hromadka II, 'Determining relative error bounds for the CVBEM', *Eng. Analysis*, **2**(2), 75–80 (1985).
15. T. V. Hromadka II, 'Variable trial functions and the CVBEM', *Numer. Methods Partial Differential Equations*, **1**, 259–278 (1985).
16. T. V. Hromadka II, 'Locating CVBEM collocation points for steady state heat transfer problems', *Eng. Analysis*, **2**(2), 100—106 (1985).
17. T. V. Hromadka II, 'Modeling steady-state advective contaminant transport by the CVBEM', *Eng. Analysis*, **3**(1), 9–15 (1986).
18. C. C. Yen and T. V. Hromadka II, 'The complex variable boundary element method in groundwater contaminant transport', in G. Yagawa and S. N. Alturi (eds), *Proceedings of the International Conference on Computational Mechanics (ICCM86 Tokyo)*, Springer, New York, 1986, pp. XI-137–XI-142.
19. T. V. Hromadka, 'Predicting two-dimensional steady-state soil freezing fronts using the CVBEM', *ASME J. Heat Transfer*, **108**, 235–237 (1986).
20. C. Lai, 'Analysis of stratified flow by the complex-variable boundary-element method', in G. Yagawa and S. N. Alturi (eds), *Proceedings of the International Conference on Computational Mechanics (ICCM86 Tokyo)*, Springer, New York, 1986, pp. XI-149–XI-154.
21. A. J. Kassab, 'The application of the complex variable boundary element method to the solution of heat conduction problems in multiply connected domains', *Ph.D. Dissertation*, University of Florida, 1989.
22. A. J. Kassab and C. K. Hsieh, 'Application of the complex variable boundary element method to solving potential problems in doubly connected domains', *Int. j. numer. methods eng.*, **29**, 161–179 (1990).
23. C. K. Hsieh and A. J. Kassab, 'Complex variable boundary element methods for the solution of potential problems in simply and multiply connected domains', *Comput. Methods Appl. Mech. Eng.*, **86**, 189–213 (1991).
24. R. R. Harryman III, T. V. Hromadka II, J. L. Vaughn and D. P. Watson, 'The CVBEM for multiply connected domains using a linear trial function', *Appl. Math. Modelling*, **14**, 104–108 (1990).
25. T. V. Hromadka II, 'Application of the CVBEM to multiply connected regions', *Appl. Math. Modelling*, **14**, 212–216 (1990).
26. M. Mokry, 'Complex variable boundary element method for external potential flows', 28th Aerospace Sciences Meeting, AIAA-90-0127, 1990.
27. D. Homentcovschi and L. Kreindler, 'The CVBEM based on a cubic spline trial function', *Eng. Analysis*, **5**(3), 161–165 (1988).
28. G. T. Symm, 'An integral equation method in conformal mapping', *Numer. Math.*, **9**, 250–258 (1966).
29. R. T. Bailey,, 'Extensions and refinements to the complex variable boundary element method including its application to numerical grid generation', *Ph.D. Dissertation*, University of Florida, Gainesville, 1991.
30. K. A. Hoffmann, *Computational Fluid Dynamics for Engineers*, Engineering Education System, Austin, Texas, 1989.
31. D. A. Anderson, J. C. Tannehill and R. H. Pletcher, *Computational Fluid Mechanics and Heat Transfer*, Hemisphere, Washington, DC, 1984.
32. R. T. Bailey and C. K. Hsieh, 'Treatment of corners in the complex variable boundary element method', in C. A. Brebbia and G. S. Gipson (eds), *Proceedings of the 13th International Conference on Boundary Elements*, Computational Mechanics Publications, Southampton and Boston, 1991, pp. 3–14.